AFRL-VA-WP-TP-2006-301

FLIGHT PATH ANGLE DYNAMICS OF AIR-BREATHING HYPERSONIC VEHICLES (PREPRINT)

Michael A. Bolender
David B. Doman

DECEMBER 2005

Approved for public release; distribution is unlimited.

STINFO FINAL REPORT

AIR VEHICLES DIRECTORATE
AIR FORCE RESEARCH LABORATORY
AIR FORCE MATERIEL COMMAND
WRIGHT-PATTERSON AIR FORCE BASE, OH 45433-7542

NOTICE

Using Government drawings, specifications, or other data included in this document for any purpose other than Government procurement does not in any way obligate the U.S. Government. The fact that the Government formulated or supplied the drawings, specifications, or other data does not license the holder or any other person or corporation; or convey any rights or permission to manufacture, use, or sell any patented invention that may relate to them.

This report was cleared for public release by the Air Force Research Laboratory Wright Site (AFRL/WS) Public Affairs Office (PAO) and is releasable to the National Technical Information Service (NTIS). It will be available to the general public, including foreign nationals.

PAO Case Number: AFRL/WS-06-0035, 4 Jan 2006.

THIS TECHNICAL REPORT IS APPROVED FOR PUBLICATION.

/s/

Michael A. Bolender
Aerospace Engineer
Control Design and Analysis Branch
Air Force Research Laboratory
Air Vehicles Directorate

/s /

Deborah S. Grismer
Chief
Control Design and Analysis Branch
Air Force Research Laboratory
Air Vehicles Directorate

/s/

Brian W. Van Vliet
Chief
Control Sciences Division
Air Force Research Laboratory
Air Vehicles Directorate

This report is published in the interest of scientific and technical information exchange and its publication does not constitute the Government's approval or disapproval of its ideas or findings.

REPORT DOCUMENTATION PAGE

Form Approved
OMB No. 0704-0188

1. REPORT DATE *(DD-MM-YY)*	2. REPORT TYPE	3. DATES COVERED *(From - To)*
December 2005	Conference Paper Preprint	12/01/2004 – 12/01/2005

4. TITLE AND SUBTITLE
FLIGHT PATH ANGLE DYNAMICS OF AIR-BREATHING HYPERSONIC VEHICLES (PREPRINT)

5a. CONTRACT NUMBER
In-house

5b. GRANT NUMBER

5c. PROGRAM ELEMENT NUMBER
N/A

6. AUTHOR(S)
Michael A. Bolender and David B. Doman

5d. PROJECT NUMBER
N/A

5e. TASK NUMBER
N/A

5f. WORK UNIT NUMBER
N/A

7. PERFORMING ORGANIZATION NAME(S) AND ADDRESS(ES)

Control Design and Analysis Branch (AFRL/VACA)
Control Sciences Division
Air Vehicles Directorate
Air Force Research Laboratory, Air Force Materiel Command
Wright-Patterson AFB, OH 45433-7542

8. PERFORMING ORGANIZATION REPORT NUMBER
AFRL-VA-WP-TP-2006-301

9. SPONSORING/MONITORING AGENCY NAME(S) AND ADDRESS(ES)

Air Vehicles Directorate
Air Force Research Laboratory
Air Force Materiel Command
Wright-Patterson Air Force Base, OH 45433-7542

10. SPONSORING/MONITORING AGENCY ACRONYM(S)
AFRL/VACA

11. SPONSORING/MONITORING AGENCY REPORT NUMBER(S)
AFRL-VA-WP-TP-2006-301

12. DISTRIBUTION/AVAILABILITY STATEMENT
Approved for public release; distribution is unlimited.

13. SUPPLEMENTARY NOTES
Conference paper preprint to be presented at the 2006 AIAA Guidance, Navigation, and Control Conference, 24 Aug 06, Keystone, CO. This report contains color.

14. ABSTRACT

The flight path dynamics of aircraft are often characterized by the presence of a right-half plane zero in the elevator-to-flight path angle transfer function. For most aircraft, the frequency of this zero is high enough that it does not limit the bandwidth of the flight control system. This is not the case, however, with air-breathing hypersonic aircraft. This class of aircraft is characterized by unstable longitudinal dynamics, strong loop interactions, and the presence of non-minimum phase transmission zeros. In the case of flight-path angle and velocity control, the presence of a low frequency transmission zero severely limits the achievable bandwidth. We show that the frequency of the zero is related to the instantaneous center-of-rotation of the aircraft, which is dependent upon the amount of lift produced by the longitudinal control effectors. In order to improve flight-path control, we investigate the feasibility of an aircraft configured with redundant pitch control effectors. The additional effector moves the instantaneous center-of-rotation, and as a result, the location of the zero. The trade-off is that the path-attitude decoupling inherent in hypersonic aircraft becomes more pronounced. Results are given for both a rigid hypersonic aircraft model and a model that includes the effects of the first fuselage bending mode.

15. SUBJECT TERMS
Aircraft Dynamics, Flight Control, Hypersonic Aircraft

16. SECURITY CLASSIFICATION OF:			17. LIMITATION OF ABSTRACT:	18. NUMBER OF PAGES	19a. NAME OF RESPONSIBLE PERSON (Monitor)
a. REPORT	b. ABSTRACT	c. THIS PAGE			Michael A. Bolender
Unclassified	Unclassified	Unclassified	SAR	40	19b. TELEPHONE NUMBER *(Include Area Code)* (937) 255-8494

Standard Form 298 (Rev. 8-98)
Prescribed by ANSI Std. Z39-18

Flight Path Angle Dynamics of Air-breathing Hypersonic Vehicles

Michael A. Bolender *
David B. Doman †
Air Force Research Laboratory, Wright-Patterson AFB, OH 45433

Abstract

The flight path dynamics of aircraft are often characterized by the presence of a right-half plane zero in the elevator-to-flight path angle transfer function. For most aircraft, the frequency of this zero is high enough that it does not limit the bandwidth of the flight control system. This is not the case, however, with air-breathing hypersonic aircraft. This class of aircraft is characterized by unstable longitudinal dynamics, strong loop interactions, and the presence of non-minimum phase transmission zeros. In the case of flight-path angle and velocity control, the presence of a low frequency transmission zero severely limits the achievable bandwidth. We show that the frequency of the zero is related to the instantaneous center-of-rotation of the aircraft, which is dependent upon the amount of lift produced by the longitudinal control effectors. In order to improve flight-path control, we investigate the feasibility of an aircraft configured with redundant pitch control effectors. The additional effector moves the instantaneous center-of-rotation, and as a result, the location of the zero. The trade-off is that the path-attitude decoupling inherent in hypersonic aircraft becomes more pronounced. Results are given for both a rigid hypersonic aircraft model and a model that includes the effects of the first fuselage bending mode.

Introduction

The control of air-breathing hypersonic aircraft poses a set of unique challenges. This class of aircraft is designed to operate over a range of flight conditions from low subsonic speeds on approach and landing to flight at high Mach numbers ($M > 10$) in the uppermost part of the earth's atmosphere. To fly through these vastly different speed regimes, a combined cycle engine will likely be necessary to achieve optimum performance. In the supersonic

*Aerospace Engineer. Senior Member AIAA.
†Senior Aerospace Engineer. Associate Fellow AIAA.

PREPRINT

speed range, the aircraft will be powered by a ramjet cycle engine. Beginning at approximately Mach 6 and up to approximately Mach 15, the engine will transition to a supersonic combustion ramjet (scramjet) cycle. As Mach Number increases, the pressure and temperature increases that occur when the flow is slowed to subsonic speed significantly reduces the performance of the ramjet; therefore, the scramjet cycle is necessary above Mach 5 or 6.

A survey of air-breathing hypersonic aircraft designs from the 1960's to the present day shows that scramjet engines are highly integrated with the airframe of the vehicle. If the engines were mounted on pods as is done with today's commercial airliners, the drag of the nacelle and supporting structure would exceed the thrust produced by the engine. An "integrated" vehicle is designed such that the forward fuselage is comprised of several "ramps" in series. Each ramp generates an oblique shock wave that compresses the air prior to entering the inlet. Thus the forward fuselage can be tailored to provide the appropriate amount of compression to the engine at the design flight condition. The pressure rise due to the forebody compression produces lift on the vehicle in addition to a nose up pitching moment. The aft fuselage is designed to act as the upper half of an expansion nozzle. The pressure of the exhaust gas acting on the aft fuselage increases the lift on the vehicle and adds a small nose down pitching moment. Thus, the propulsion system plays an important role in the stability and control characteristics of the vehicle since the aerodynamic forces and moments are dependent not only upon the Mach number, angle-of-attack, and sideslip angle, but also upon the engine power setting. In addition, performance of the scramjet is now dependent upon the angle-of-attack, Mach number, and power setting. The angle-of-attack and Mach number determine the amount of airflow that the engine receives. This is because the capture area and the amount of spilled airflow are functions of angle-of-attack and Mach number. The performance of the scramjet is also dependent upon the amount of compression that the forebody delivers and thus is also a function of Mach and angle-of-attack. Because the scramjet engine is located on the bottom of the aircraft, the thrust vector offset from the center-of-mass will contribute a nose-up pitching moment that must

be countered by the elevator or some other longitudinal control effector.

Previous work by Schmidt[1] concluded that an integrated flight-propulsion control system is necessary to control this class of vehicle. Schmidt also showed that control synthesis is difficult due the fact that the plant is unstable with non-minimum phase transmission zeros, there exists significant cross-coupling between the inputs and outputs, and the plant model possesses significant modeling uncertainty near the gain crossover frequency. Schmidt's conclusions were based on the linearized dynamics of a simplified model of the longitudinal dynamics of an air-breathing hypersonic vehicle.[2] More recently, Bolender and Doman[3] developed a non-linear model of an air-breathing hypersonic aircraft similar to that of Chavez and Schmidt[2] that exhibits the same qualitative characteristics as above.

The longitudinal dynamics of hypersonic aircraft differ from those of subsonic aircraft. There is a readily identifiable short-period mode that corresponds to the classical definition, but the similarities end there. In addition, there is a phugoid mode that is independent of speed[4] and a height mode that is dependent upon $\partial T/\partial M$ and $\partial T/\partial h$.[5] The height mode is generally neglected in the dynamics of conventional, subsonic aircraft.

Also, another important difference between hypersonic and conventional aircraft occurs with the relationship between the flight path and pitch attitude of the vehicle. For supersonic and hypersonic aircraft, path-attitude decoupling[6] is prevalent. The implication of this is that there is an increased lag in the flight path angle relative to the pitch angle for a given elevator input. The flying quality metric that determines the lag between the pitch angle and flight path angle is the "T_{θ_2} zero". For conventional, low speed aircraft, the lag between the flight path angle and the pitch attitude is not readily apparent. For example, the LearJet[7] has a T_{θ_2} of approximately 1.57 sec at 40,000 ft and Mach 0.7 while the XB-70 has a $T_{\theta_2} \approx 4.81$ s at Mach 3.0 and 60,000 ft.[8] Sachs[6] derives a physically realizable upper limit on T_{θ_2} of approximately 27 s for hypersonic aircraft and shows that the increase in T_{θ_2} is due the density gradient of the atmosphere and the aircraft's speed. In comparison, Mil-STD-1797[9] guidance suggests that for Level 1 flying qualities, $1/T_{\theta_2} \geq 0.28$ (or equivalently

$T_{\theta_2} \leq 3.57$ sec) for a Class III aircraft. In a companion paper, Sachs[10] shows that the T_{θ_1} and T_{θ_2} zeros couple whenever the flight speed of the aircraft is greater than some threshold speed that is dependent upon the lift curve slope and the lift of the vehicle. The consequence is that there is no correlation between n_z/α and $1/T_{\theta_2}$.

Altitude stability is another problem unique to high speed that has been studied.[5] Given the velocities at which hypersonic aircraft travel, a small perturbation in the flight path angle can result in large changes in altitude. Stengel[5] discusses the dependence of altitude stability on the phugoid and height modes and shows that if M_u, the speed stability derivative, is only a function of the thrust offset, then the height mode time constant increases. In a separate study, Bloy[11] shows that the amount of thrust offset indirectly affects dynamic stability through the speed stability derivative, and when the thrust vector is below the center-of-mass, the phugoid damping is reduced.

Handling qualities requirements for manned hypersonic aircraft have been addressed in References [12–14]. The reports by Berry[12,13] discuss requirements definitions studies and identify what flying qualities specification would need to be changed to make them applicable to hypersonic aircraft. On the other hand, McRuer, et.al.[14] discussed stability and control issues in addition to flying qualities deficiencies based on a study of data available at the time. They cited model uncertainty as a major issue and recommended that flying quality level designations be tied to uncertainties in the aircraft and control system. Specific recommendations were only given for the power-off approach and landing phase.

Vu and Biezad[15] studied the effects of a direct-lift flap on the GHAME hypersonic model. They cited an increase in T_{θ_2} in the hypersonic speed regime as motivation for improving the $\gamma(s)/\theta(s)$ response. The control system designed by Vu and Biezad was a G-command control system with "alpha follow-up" and was designed based upon the short period dynamics of the aircraft. The direct-lift flap deflection was connected to the elevon deflection via an interconnect gain. Their control design approach was then validated in a pilot-in-the-loop simulation to determine handling qualities, and received favorable ratings from the

test pilot. Vu and Biezad also argue that the an appropriate handling qualities metric for hypersonic aircraft should be based on the bandwidth of the flight path angle, ω_{BW_γ} of the $\gamma(s)/\delta_s$ transfer function (δ_s is the pilot stick input), although they fail to give any specific recommendation.

In this paper, we will address the effects of vehicle configuration on the available bandwidth of the open-loop aircraft dynamics. Specifically, we are interested the response of the aircraft to changes in flight path angle and velocity. We will show that for a typical configuration of an air-breathing hypersonic vehicle, where the control inputs are elevator and throttle, that the response is non-minimum phase and bandwidth limited due to the location of the right-half plane transmission zero. Subsequently, an alternate configuration will be proposed and analyzed to show that by changing the configuration of the vehicle, the bandwidth of the system can be improved.

Problem Statement

Outer loop control of aircraft is done by a pilot or flight management system using velocity and flight path angle as the controlled variables. In subsonic aircraft the two loops are controlled using throttle and the elevator respectively when operating on the front-side of the power-required curve. Since the engines are not integrated with the airframe to the degree that they are on hypersonic aircraft, the design of the two control loops can be considered independently.

A vast majority of aircraft are designed with a conventional horizontal tail that uses an elevator for pitch control, with recent exceptions being the delta-wing/canard configured fighters that were designed in Europe in the late 1980's/early 1990's. If one looks at the elevator to flight-path angle transfer function, $\gamma(s)/\delta_e(s)$, over a wide range of aircraft, one will see the presence of non-minimum phase zeros in the factored transfer function numerators. From McRuer,[16] the numerator is written as: $N^{\gamma}_{\delta_e} = (s + 1/T_{\gamma_1})(s + 1/T_{\gamma_2})(s + 1/T_{\gamma_3})$, where $1/T_{\gamma_3} = -1/T_{\gamma_2}$ are mirror image zeros about the imaginary axis for $1/T_{\gamma_3}$

A/C	Mach	Altitude	$N^{\gamma}_{\delta_e}$
F-104[8]	0.9	35Kft	$0.1138(s+.00399)(s-8.48)(s+9.18)$
Boeing 747[8]	0.8	40Kft	$0.0234(s-.00166)(s-3.64)(s+4.08)$
LearJet[7]	0.7	40Kft	$(s+0.0041)(s-13.1531)(s+13.3757)$
XB-70[8]	3.0	60Kft	$0.0071(s+0.00223)(s-8.42)(s+8.55)$
GHAME[15]	3	60Kft	0.1467(s+0.0140)(s-7.5973)(s+8.0864)
AFRL Generic HSV[3] [a]	8.0	85Kft	$0.0165(s-.0002)(s-3.4641)(s+3.5134)$

[a]This is a modified version of the aircraft model presented in Reference [3]

Table 1: Open-loop $\gamma(s)/\delta_e(s)$ Transfer Function Numerators

real. A survey of $\gamma(s)/\delta_e(s)$ zeros for several different aircraft was taken from the literature and is given in Table 1. It is worthwhile noting that the right-half plane zero in $N^{\gamma}_{\delta_e}$ is close in magnitude to the right-half plane transmission zero, and can be considered as a first approximation to the transmission zero.

The presence of the non-minimum phase zero in the δ_e to γ transfer function can be attributed to the fact that if one commands an increase in flight path angle to climb to a higher altitude, the elevator deflects trailing edge up. The lift produced by the tail instantaneously decreases, decreasing the total lift on the aircraft. At this point, the total lift is now less than the weight of the vehicle, so the aircraft will instantaneously lose altitude before achieving a positive climb rate. Also, when the elevator is deflected, the aircraft will experience a change in angle-of-attack. The angle-of-attack initially increases faster than the pitch attitude, making the flight path angle negative until $\theta > \alpha$.

Traditionally, the lag between flight path angle and pitch attitude is prescribed by imposing a lower bound on $1/T_{\theta_2}$. The pitch attitude to flight path angle transfer function is approximated by

$$\frac{\gamma(s)}{\theta(s)} = \frac{1}{T_{\theta_2}s+1} \tag{1}$$

where $T_{\theta_2} \approx mV_0/L_\alpha$. However, this approximation is valid only over the frequency range where the short-period approximation is valid because the actual $\gamma(s)/\theta(s)$ transfer is improper. For hypersonic aircraft, the T_{θ_1} and T_{θ_2} zeros can couple, making the specification of the T_{θ_2} zero difficult.

Field, et.al.[17] studied the location of the pitch instantaneous center-of-rotation on flying qualities, focusing their study on the approach and landing tasks. They showed that difficulty controlling the flight path angle during a flare maneuver is dependent upon the location of the instantaneous center-of-rotation relative to the center-of-mass, the location of the pilot relative to the center-of-rotation, and the mass properties of the aircraft. They developed a geometric criterion to correlate the location of the instantaneous center-of-rotation to the ability to control flight path in the flare. Applying the geometric criteria to the space shuttle and the Concorde, which are both high-speed, aft-engine, delta wing configurations, shows that these aircraft fall in a region that predicts they will possess flight path angle control deficiencies, susceptibility to pilot-induced oscillations, and a tendency to land short and heavy.

It is straightforward to show that there is a correspondence between the instantaneous center-of-rotation and the right-half plane zero in $N^{\gamma}_{\delta_e}$. From McRuer,[16] the zero of $N^{\gamma}_{\delta_e}$ that is of interest is given by

$$\frac{1}{T_{\gamma_3}} = \sqrt{M_\alpha - \frac{M_{\delta_e}}{Z_{\delta_e}} Z_\alpha} \tag{2}$$

From Field,[17] the instantaneous center-of-rotation relative to the center-of-gravity is approximated by $l_{cor} = Z_{\delta_e}/M_{\delta_e}$. Direct substitution into Equation 2 gives

$$\frac{1}{T_{\gamma_3}} = \sqrt{M_\alpha - \frac{Z_\alpha}{l_{cor}}} \tag{3}$$

Note that this expression assumes X_{δ_e} is zero and that $|X_u(M_{\dot{\alpha}} + M_q)| \ll |M_\alpha - M_{\delta_e} Z_\alpha / M_{\delta_e}|$. Since the dominant contribution to M_α and L_α is from the wing-body, we can see that for an aircraft with an aft-mounted, horizontal tail, $1/T_{\gamma_3}$ moves to $\sqrt{M_\alpha}$ as l_{cor} increases to infinity. The trajectory that the zero follows in the complex plane will depend upon the sign of M_α. If $M_\alpha < 0$, then lower bound for $l_{cor} > 0$ is imaginary, with the zero becoming imaginary when $l_{cor} = Z_\alpha / M_\alpha$. The zero will also be imaginary for $l_{cor} < 0$ since $Z_\alpha < 0$. This is shown in Figure 1. The case where $M_\alpha > 0$ is simply the mirror image about the y-axis.

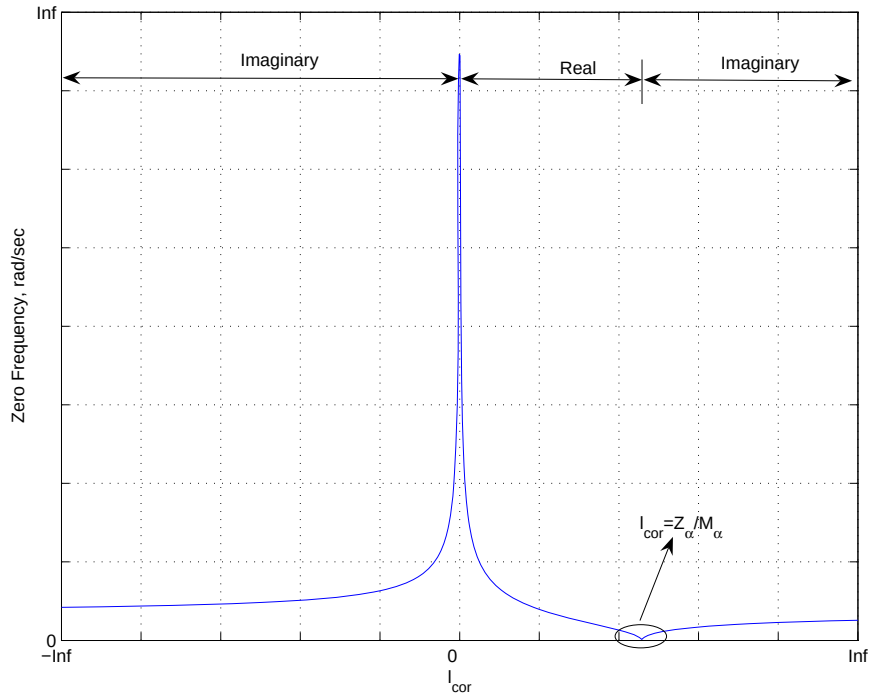

Figure 1: Zero Frequency as a Function of l_{cor}

It is interesting to note that T_{θ_2} is also a function of l_{cor}. From McRuer,[16] we have

$$\frac{1}{T_{\theta_2}} = \frac{1}{U_0}(-Z_\alpha + \frac{M_\alpha Z_{\delta_e}}{M_{\delta_e}}) \tag{4}$$

Substituting for l_{cor} gives

$$\frac{1}{T_{\theta_2}} = \frac{1}{U_0}(-Z_\alpha + M_\alpha l_{cor}) \tag{5}$$

Thus, from Equation 5, the behavior of T_{θ_2} is dependent upon the sign of M_α.

Thus $1/T_{\theta_2}$ always increases as l_{cor} increases for a statically unstable aircraft. Therefore, if the aircraft has $M_\alpha > 0$, then there will be a path-attitude decoupling that occurs as the instantaneous center-of-rotation moves to the center-of-gravity. The expressions given in Equations 3 and 5 show that the placement of $1/T_{\gamma_3}$ and $1/T_{\theta_2}$ are dependent upon the lift and pitching moment generated by the elevator. Two or more control effectors working together and capable of applying a couple on the aircraft will move l_{cor} closer to the center-of-gravity and improve the location of the $1/T_{\gamma_3}$ zero.

We are able to relate the position of the right-half plane zero of $N_{\delta_e}^{\gamma}$ to T_{θ_2} since both are functions of l_{cor}

$$\frac{1}{T_{\gamma_3}} = \sqrt{\frac{M_\alpha U_0}{U_0 + T_{\theta_2} Z_\alpha}} \tag{6}$$

Due to the coupling between the propulsion system and the aerodynamics in hypersonic aircraft, a multi-variable control design approach should be used to optimize the closed-loop dynamics. We are interested in controlling velocity and flight path angle; however, it can be shown that this transfer matrix, with elevator and throttle as the control inputs, is not diagonally dominant. Controlling velocity and flight path angle using throttle and elevator means that we will have a right-half plane transmission zero. The presence and location of this zero will limit the available bandwidth of the closed-loop control system.[18] The presence of an unstable pole places a lower bound on the bandwidth since it must be greater than the frequency of the unstable pole.[18] The bounds on the bandwidth won't limit the closed-loop performance if there is sufficient frequency separation between the pole and the zero. Stein[19] gives a rule-of-thumb that the bandwidth should exceed the frequency of the aircraft's unstable pole by a factor of ten. From the flight control engineer's point-of-view, the achievable control system performance is determined by real, physical constraints that arise due to the aircraft configuration. In order to improve the closed-loop performance, a change to the aircraft configuration is necessary.

The hypersonic aircraft model we will be using (see Reference [3]) is unstable with a right-half plane pole $s = 1.3121$ and a right-half plane transmission zero at $s = 3.3449$. The performance that can be achieved for this aircraft using closed-loop control is very limited, and we can't achieve the desired closed-loop performance in terms of the requirement that the bandwidth should exceed the frequency of the unstable pole by a factor of ten.

We want to show that the closed-loop performance of the hypersonic vehicle can be improved by altering the control effectors that are on the vehicle. By modifying the aircraft configuration, we are forcing the right-half plane transmission zero to move further to the right in order to provide relief for the control system design. For this paper, we are consider-

ing only one primary configuration change– the addition of a canard that is ganged with the elevator using a constant elevator-to-canard interconnect gain. We will analyze the design for the rigid aircraft for varying canard lengths, interconnect gains, and canard locations in order to determine sensitivity of the zero location due to non-linear aerodynamics. We will then show the effects of the canard on the flexible aircraft model given in Reference [3].

Hypersonic Vehicle Model

The aircraft model developed in this study was developed in-house to study flight control issues pertaining to air-breathing hypersonic vehicles.[3] The model uses quasi-steady gas dynamics to determine the pressure distribution over the vehicle. The scramjet model includes a variable area diffuser, a fixed nozzle, and a constant area combustor. The combustion process is modelled as a change in total temperature to the airflow (Rayleigh flow). The effects of the fuselage first bending mode on the aircraft dynamics are also captured in the model. The equations-of-motion for the flexible aircraft model are rather complex because they account for the effects of pitch and plunge on the flexible modes. As a result it is very difficult to gain insight into the effect of stability and control derivatives on the poles and zeros of the linearized system. For this particular study, the model was simplified to include only the rigid body modes. Two additional changes were made to the engine model. For simplicity, the diffuser area ratio was fixed to a value of unity. The second change was to use fuel equivalence ratio as the control input to the engine instead of the change in total temperature across the combustor. Numerically, this approach avoids some of the scaling problems associated with using temperature input as the control. The fuel equivalence ratio is defined as $\phi = f/\lambda$ where f is the fuel-to-air ratio and λ is the fuel-to-air ratio for stoichiometric combustion. The fuel equivalence ratio is related to the total temperature change across the combustor ($\Delta T_0 = T_{t3} - T_{t2}$) by

$$\frac{T_{t3}}{T_{t2}} = \frac{1 + \frac{H_f \eta_c \lambda \phi}{c_p T_{t2}}}{(1 + \lambda\phi)} \tag{7}$$

Open-loop Pole	ζ	ω_n
-1.44	1.0	1.44
1.31	-1.0	1.31
-1.71×10^{-3}	1.0	1.71×10^{-3}
$-1.79 \times 10^{-5} \pm 3.96 \times 10^{-2}$	4.53×10^{-4}	3.96×10^{-2}

Table 2: Open-loop Poles for Baseline Vehicle

where H_f is the lower heating value of the fuel, η_c is the combustion efficiency, c_p is the specific heat of air, T_{t2} is the total temperature at the combustor inlet, and T_{t3} is the total temperature at the combustor exit. For liquid hydrogen, typical values are $H_f = 51,500$ BTU/lbm and $c_p = 0.24$ BTU/(lbm °R). The combustion efficiency was assumed to be $\eta_c = 0.9$.

The aircraft was trimmed at an altitude of 85,000 ft and at Mach 8 and subsequently linearized about this trim condition. The open-loop poles are given in Table 2. The aircraft is open-loop unstable with two real short period poles. The altitude mode is real and stable, although at a very low frequency. The phugoid mode is also stable, but again it is a slow mode and is very lightly damped due to the fact that the engine and thrust line-of-action is below the center-of-gravity. The transmission zeros for the 2×2 transfer matrix defined by $\boldsymbol{y} = \begin{bmatrix} \gamma & V \end{bmatrix}^T$ and $\boldsymbol{u} = \begin{bmatrix} \delta_e & \phi \end{bmatrix}^T$ are 0, -3.3954, and 3.3449. Note that there are three finite transmission zeros, two that lie on the real axis and the third at the origin. The zero at the origin corresponds to the kinematic relation $\dot{h} = V_t \sin\gamma$.

Canard Configured HSV

In this section, we propose and investigate a configuration change to the hypersonic aircraft that will move the right-half plane transmission zero further to the right. This is done in order to increase the available bandwidth for the control design. The proposed design change is the addition of a canard to the aircraft. The canard will work in conjunction with the elevator through an interconnect gain. By selecting an appropriate gain and canard size, l_{cor} is moved closer to the center-of-gravity. This occurs because L_{δ_e} is reduced while

M_{δ_e} is increased. The pitching moment that is applied to the aircraft by deflecting the control surfaces is now almost a couple, which improves the speed of the θ response. We will first study the rigid aircraft, then we will apply our design to the flexible aircraft model to investigate the effects of the configuration change on the transmission zeros of the linearized system.

For our hypersonic aircraft model, the selection of the interconnect gain is not trivial due to the inherent coupling present in the system. From Equation 2, we know that the position of the $1/T_{\gamma_3}$ is dependent upon the instantaneous center-of-rotation $l_{COR} = Z_{\delta_e}/M_{\delta_e}$. Since the canard and elevator are connected by a static gain, we can consider their effects to be additive. Therefore, we can write the instantaneous center-of-rotation as:

$$l_{COR} = \frac{Z_{\delta_e} + kZ_{\delta_c}}{M_{\delta_e} + kM_{\delta_c}} \tag{8}$$

Ideally, we use the canard to place the instantaneous center-of-rotation at the center-of-gravity in order to drive the zero to infinity. Thus, if we equate the numerator of $l_{COR} = 0$, then the ideal interconnect gain is given by

$$k_{opt} = -\frac{Z_{\delta_e}}{Z_{\delta_c}} = -\frac{L_{\delta_e}}{L_{\delta_c}} \tag{9}$$

The gain k_{opt} sets the deflection of the canard such that it exactly cancels the lift due to the elevator.

When considering the hypersonic vehicle, or any vehicle for that matter, we have a much more daunting task. The lift due to the control effectors is in general a non-linear function of deflection, angle-of-attack, and Mach number. The interconnect gain to keep l_{COR} at the center-of-gravity is therefore dependent upon the flight condition and deflection. This implies that a static gain, while valid in the neighborhood of the trim condition, is not valid over the entire flight envelope, and dynamic scheduling of the interconnect gain is required to maintain the location of the instantaneous center-of-rotation. The constraint for the instantaneous center-of-rotation for the non-linear expression now becomes $L(\delta_e, \boldsymbol{P}) + L(\delta_c, \boldsymbol{P}) = 0$, where $\boldsymbol{P}$ is a vector of parameters such as Mach and angle-of-attack that

uniquely define the lift due to the control effectors. If we assume that $\delta_c = k\delta_e$, then

$$L(\delta_e) + L(k\delta_c) = 0 \tag{10}$$

at a given flight condition. One way to ensure the lift constraint is satisfied is through the use of control allocation. Using control allocation, we will not need to solve for the gain that will satisfy the lift constraint explicitly. Instead the control allocation finds the deflections that satisfy the constraint and gives the desired controlled variable, if there exists a solution to the control allocation problem. The approach of using control allocation to dynamically place the system transmission zeros is currently an area of active research.

The configuration study that we undertook considered the effects of the canard mean aerodynamic chord length and the canard-elevator interconnect gain on the transmission zeros of the $[\gamma(s)\ V_T(s)]$ to $[\delta_e\ \delta_\phi]$ transfer matrix. The canard length was varied from 3 ft to 15 ft and the elevator-canard interconnect gain varied from -2.5 to -1.5. The canard is deflected in the direction opposite to the elevator with the intent of cancelling the lift produced by the elevator. The net result is that we reduce the effective L_{δ_e} while increasing M_{δ_e}. This subsequently moves the location of the instantaneous center-of-rotation, and as a result, the right-half plane zero in $N^{\gamma}_{\delta_e}$ and the right-half plane transmission zero of the system matrix.

The pole/zero maps for interconnect gains of -1.5, -2.0 and -2.5 are shown in Figures 2-4. Note that the general trend is for the two real transmission zeros to move away from the imaginary axis and then break into a stable, albeit a lightly-damped, complex-conjugate pair. The frequency of the right-half plane transmission zero, as a function of canard length, is shown in Figure 5 for varying interconnect gains and clearly illustrates this behavior. Note that for each curve in Figure 5, there is a peak frequency that occurs when the instantaneous center-of-rotation is located at the center-of-mass (i.e.,, $l_{COR} = 0.$) As the instantaneous center-of-rotation is moved just behind the center-of-mass, the zero will move to the imaginary axis because the ratio $-Z_\alpha/l_{COR} < 0$ dominates M_α in Equation 3. Ideally, in a purely linear system, stable transmission zeros are desired, as this allows the

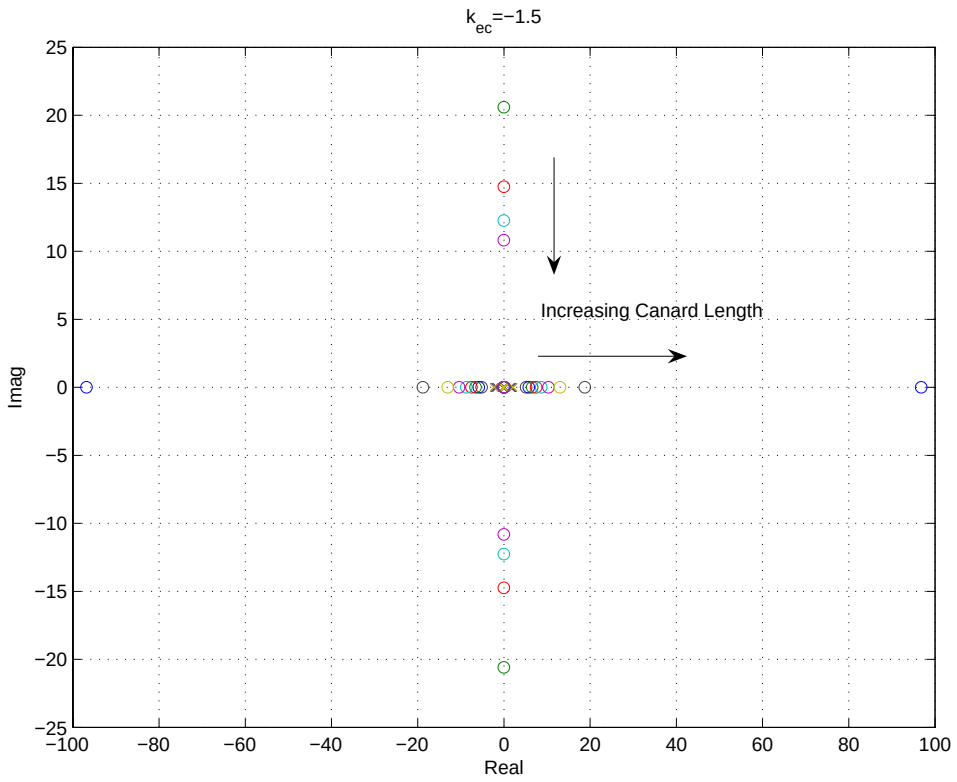

Figure 2: Pole/Transmission Zero Map for Interconnect Gain = -1.5

upper limit on the system bandwidth to be selected arbitrarily.

Figure 6 shows the effect of a fixed canard length and a varying interconnect gain on the location of the right-half plane transmission zero. We chose a canard length of 7 ft and varied the interconnect gain from -2.5 to -1.5 in steps of 0.25. The plot again shows that the two real transmission zeros break into a very lightly damped complex conjugate pair at some interconnect gain between -3 and -2.75 that corresponds to the condition that $l_{COR} = 0$. Therefore, based on the performance requirements, the canard sizing and the interconnect gain can be selected to give optimum performance for a given flight condition. Any uncertainty due to modeling error at a given flight condition will likely not have a drastic effect on the zero location.

Finally, the effect of the canard position on the transmission zeros is shown in Figure 7. The canard chord length is fixed at 10 ft, and the interconnect gain between the rudder and the canard is fixed at -1.5. In Figure 7 we see that the optimum location for the placement

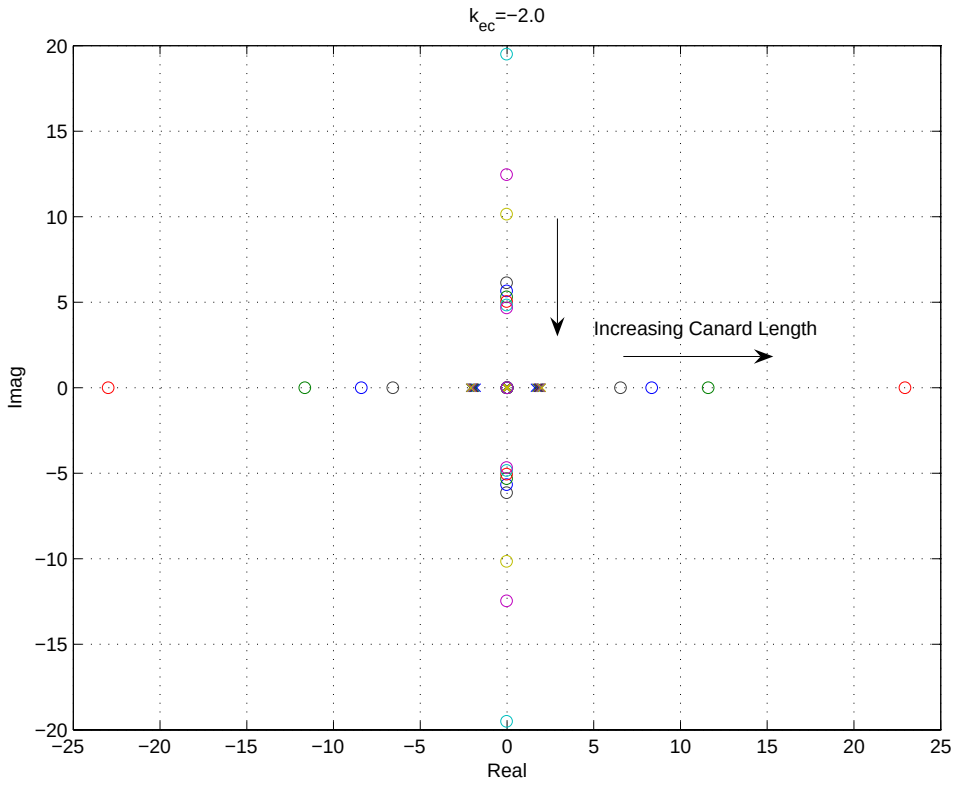

Figure 3: Pole/Transmission Zero Map for Interconnect Gain = -2.0

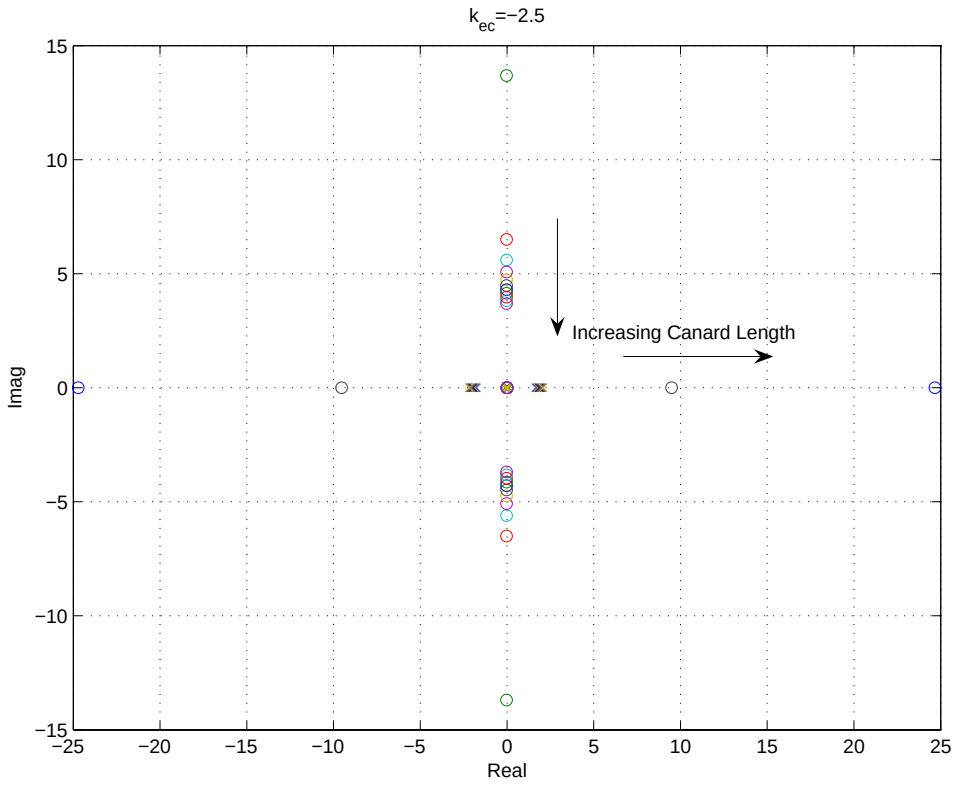

Figure 4: Pole/Transmission Zero Map for Interconnect Gain = -2.5

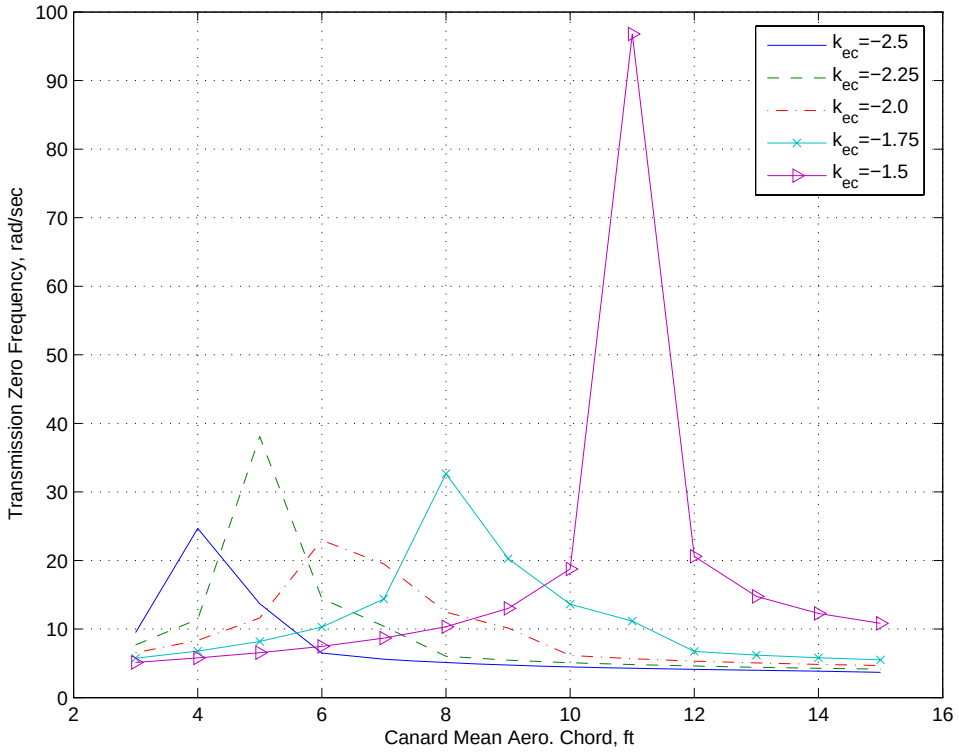

Figure 5: Right-half Plane Transmission Zero Frequency as a Function of Canard Length for Varying Elevator/Canard Interconnect Gains

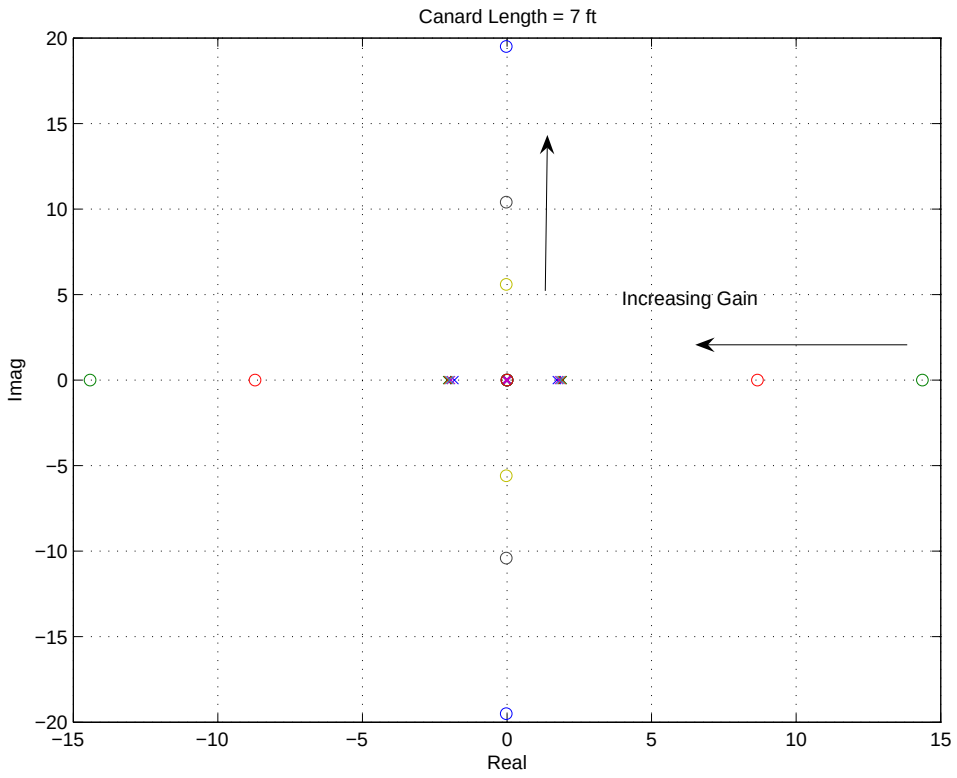

Figure 6: Pole/Transmission Zero Map as a Function of Elevator/Canard Interconnect Gain

of the control effector for this particular gain is 45 ft behind the nose of the aircraft (positive is measured forward out the nose). Figure 7 indicates that a direct-lift flap may improve the system response (see Vu and Biezad[15]), but is not optimal.

Effects on the Flexible Aircraft

Due to flexibility effects, we expect that the coupling of the structural dynamics with the rigid body dynamics will alter the structure of the pole-zero map. In fact, for the linearized dynamics of the nominal, flexible aircraft, we have a significant change in the derivatives Z_{δ_e} and M_{δ_e}. The flexibility effects not only change the sign of M_{δ_e} such that a positive elevator (trailing edge down) produces a positive moment (nose-up), the magnitude of the derivative is almost seven times as large as that on the rigid aircraft. The lift produced by the elevator is increased by an order of magnitude. Thus we can conclude that the inclusion of the structural dynamics have a significant impact on the linearized plant. While

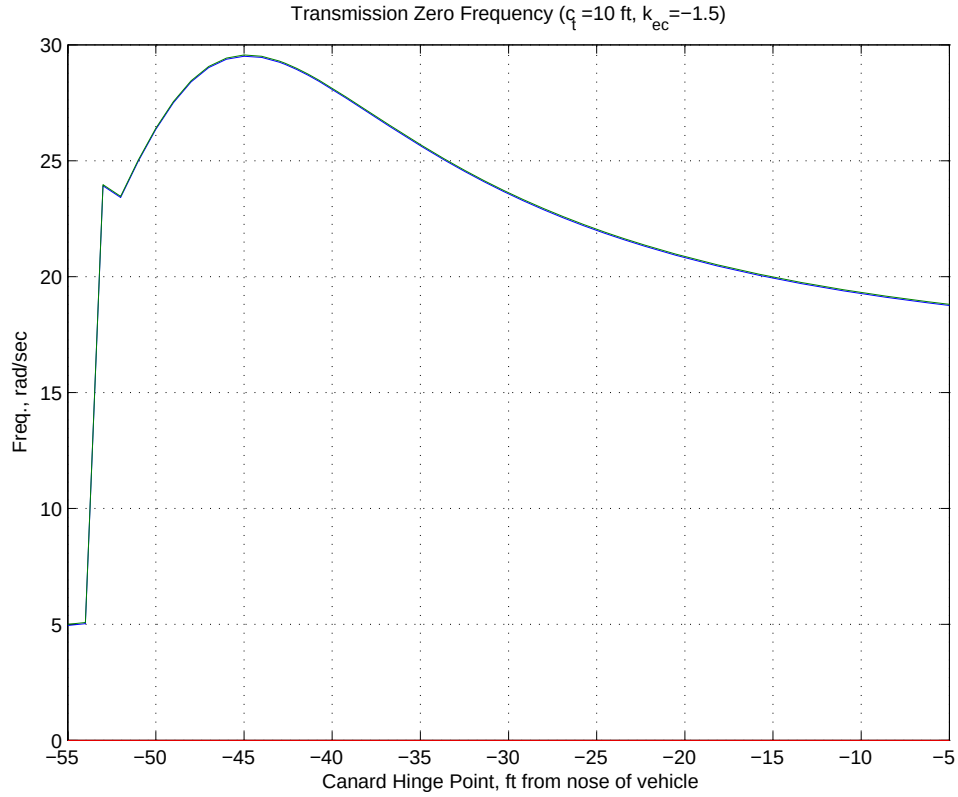

Figure 7: Transmission Zero Frequency as a Function of Canard Position

perturbations in the elastic aircraft stability and control derivatives were expected, the magnitude of the changes that we are seeing were not. Thus, it becomes much harder to select an interconnect gain for the flexible aircraft due to the added flexibility effects of the structure and the dependence of the elevator and canard effectiveness on the deflection of the fuselage. While we could easily predict the behavior of the zeros in the rigid case, we cannot do so given the complex structure of not just the non-linear equations-of-motion, but the linearized equations as well. Therefore, in the absence of a set of tractable linearized equations, we are left with a purely numerical exercise to perform for the flexible aircraft. Note however, that altering the structural model to something simpler (e.g., by ensuring that the flexible modes are inertially decoupled from the rigid-body modes) the results would be more tractable analytically.

In Figure 8, the pole-zero locations are shown for the hypersonic aircraft model given in Reference [3] at the same flight condition as given above for the rigid aircraft. The rotation of the elevator hinge point with the structure reduces elevator effectiveness when the rotation of the aft fuselage deflects upward since the apparent angle-of-attack is reduced. Since the instantaneous center-of-rotation is the ratio $Z_{\delta_e}/M_{\delta_e}$, there is not a significant change in its location due to this effect. For the baseline flexible aircraft, the instantaneous center-of-rotation is $l_{COR} = 57$ ft, so the transmission zeros are essentially unchanged from the values we saw previously with the rigid aircraft. However, the set of transmission zeros now includes two pairs of complex-conjugate transmission zeros that are mirrored about the imaginary axis. These transmission zeros are those associated with the free vibration of the aircraft's fuselage. Since the "actuator" and the "sensor" are not collocated, the transmission zeros mirror each other about the $j\omega$ axis. These particular right-half plane transmission zeros are not limiting the bandwidth in a practical sense since they have a natural frequency of 16 rad/sec, which is greater than 10 times the unstable pole at 1.39 rad/sec.

As a result of the added complexity, when the canard is added to the vehicle, we see a much more complex distribution of the transmission zeros. The pole/zero maps for the same

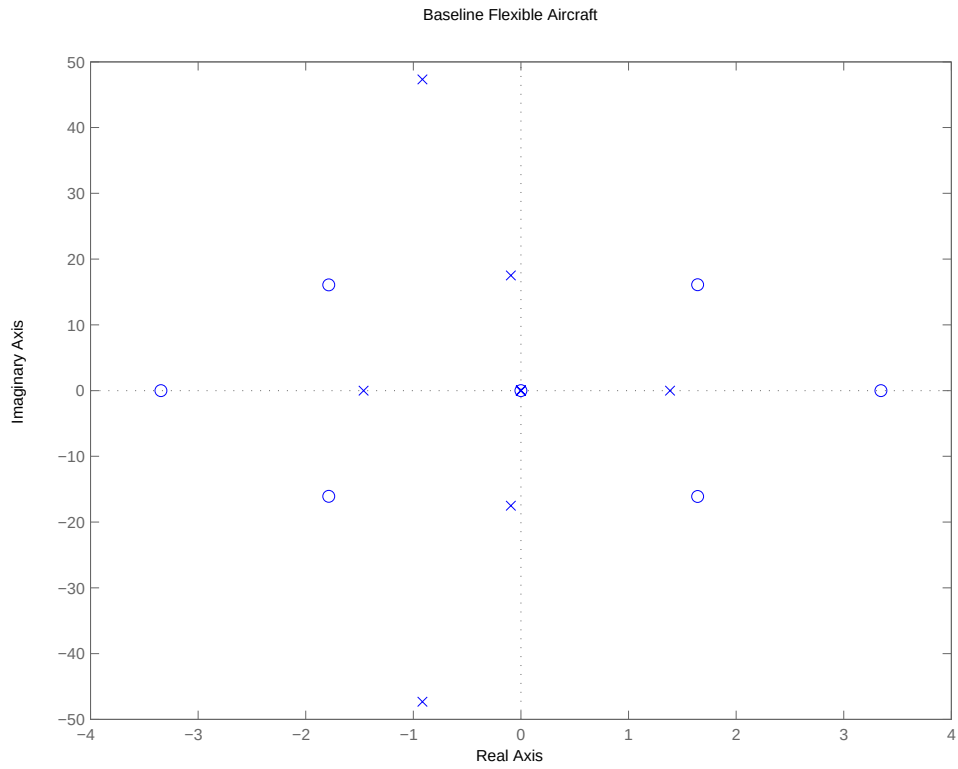

Figure 8: Pole/Zero Map of Baseline Flexible Aircraft

gains and canard lengths as for the rigid aircraft example are shown in Figures 9-11. For the most part, the real transmission zeros couple with the structural modes and split into a complex conjugate pair. What is readily apparent is that in most cases, the amount of bandwidth that can be added by moving the instantaneous center-of-rotation is limited. Like the elevator, the force generated by the canard is not only a function of the deflection and the angle-of-attack, it is also dependent upon the rotation of the forebody. The deflection of the forebody is in turn dependent upon the amount of force generated by the canard. The tendency will be for the deflection angle of the forward fuselage to be reduced at a trim condition since the canard will apply a force in the positive z direction in order to apply a nose-down pitching moment (recall that we are using the canard in conjunction with the elevator in order to apply a couple to the aircraft.) In fact, if the canard down force is large enough, the mode shape of the aircraft will become anti-symmetric as the concavity of the deflection curves for the fore and aft beams will differ. The center-of-mass will be

an inflection point and the maximum deflection will remain at each end of the fuselage. The situation will become more complicated as additional mode shapes are included in the model. The position of sensors and actuators relative to, not only one another, but also the nodal points, is known to have an effect of the position of the transmission zeros.[20] Therefore, filtering the sensors is necessary in order to mitigate these unwanted effects.

Figures 12 and 13 show how the transmission zero frequencies vary as the canard position is moved from the nose of the aircraft close to the center-of-mass. Compared with the baseline aircraft, the real transmission zeros have become complex conjugate pairs that are now coupled with the structural zeros. Note that the change in frequency as the canard moves is not as large as was seen in the rigid aircraft. Again, including more mode shapes into the model may affect the movement of the right-half plane zeros.

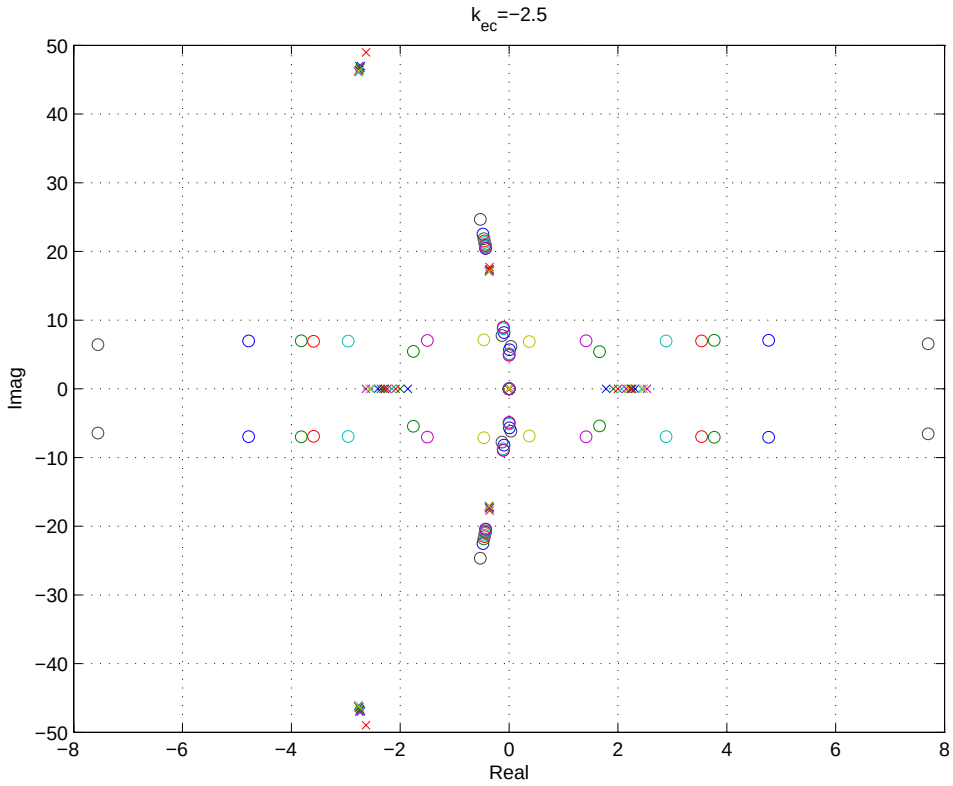

Figure 9: Pole/Zero Map of Flexible Aircraft with Canard and Interconnect Gain $k_{ec} = -2.5$.

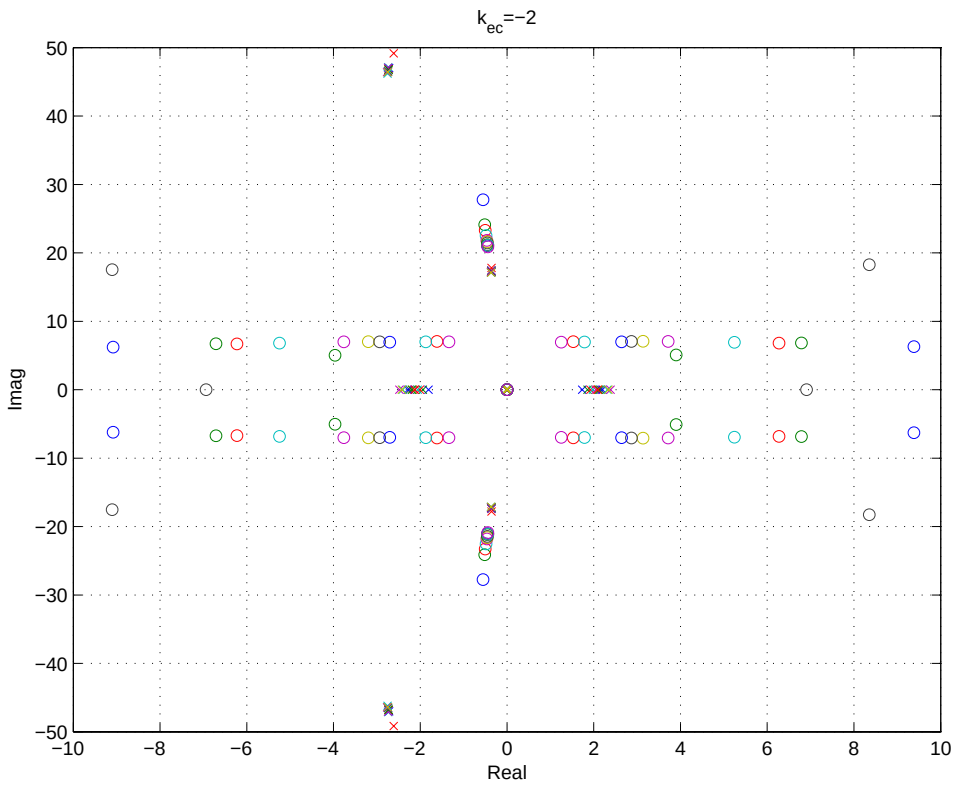

Figure 10: Pole/Zero Map of Flexible Aircraft with Canard and Interconnect Gain $k_{ec} = -2$.

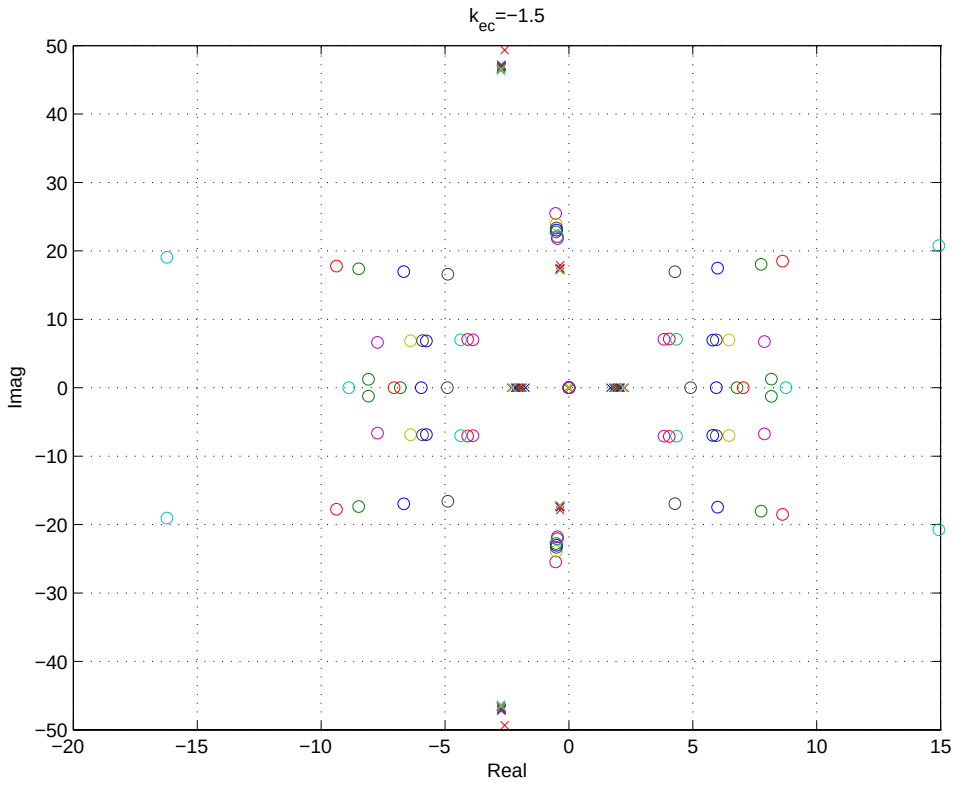

Figure 11: Pole/Zero Map of Flexible Aircraft with Canard and Interconnect Gain $k_{ec} = -1.5$.

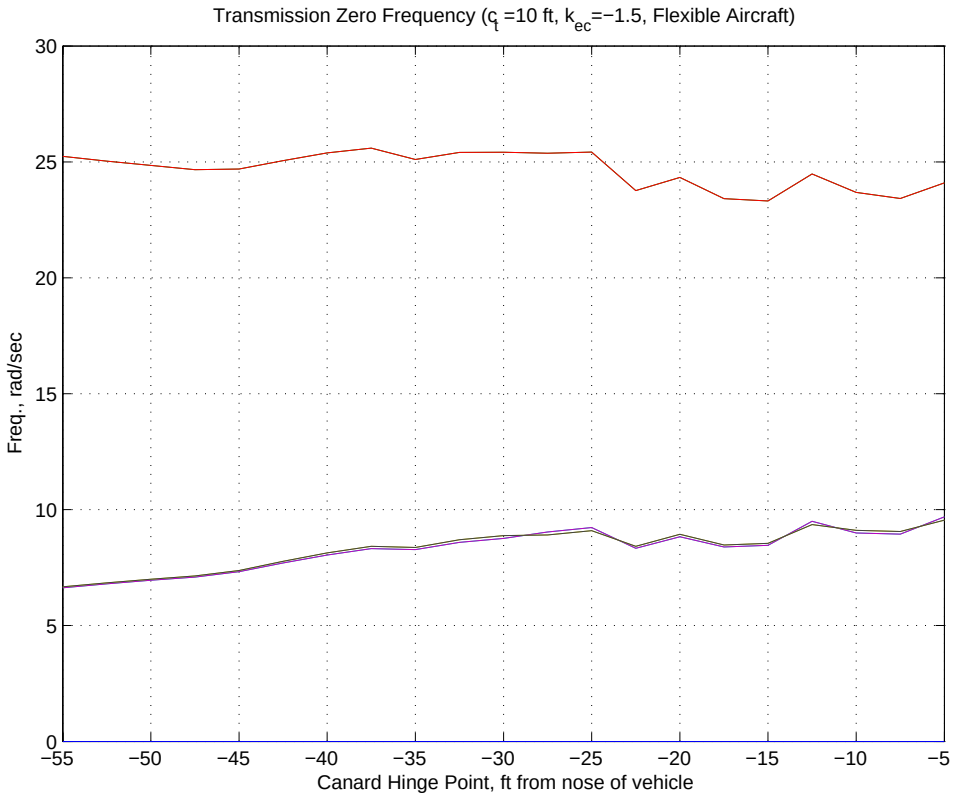

Figure 12: Transmission Zero Frequency as a Function of Canard Position

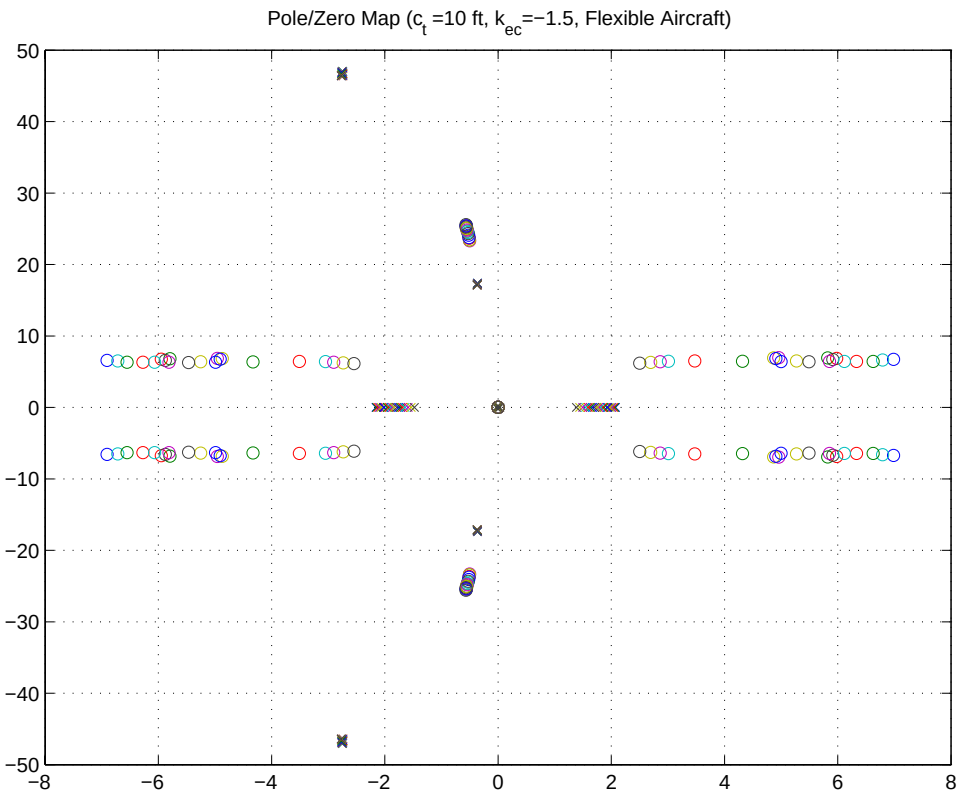

Figure 13: Pole/Zero Variation as a Function of Canard Position

Conclusions

The control of air-breathing hypersonic aircraft is a difficult problem because the aircraft are typically dynamically unstable, have a high-degree of loop interaction, and exhibit non-minimum phase behavior. In particular, the performance that can be achieved by a single-input single-output control system that regulates the flight-path angle is impacted by the presence of a low frequency, right-half plane zero in the elevator-to-flight-path angle transfer function. In the multi-variable case where the inputs are elevator and equivalence ratio and the outputs are flight-path angle and velocity, there is a right-half plane transmission zero of approximately the same frequency as the right-half plane zero of $N^{\gamma}_{\delta_e}$. It is shown that the zeros are functions of the instantaneous center-of-rotation for the rigid-body case. In order to locate the right-half plane zero at a more desirable location, we then investigated the

effects of adding an additional control surface for pitch control. The additional effector was ganged with the elevator and it was shown that there is an optimum inter-connect gain that will exactly cancel the lift produced by the elevator. In the case where the lift of the elevator is exactly cancelled by the lift of the canard, the zero will move to infinity. A mismatched gain will move the instantaneous center-of-rotation closer to the center-of-mass, resulting in a zero that is further to the right as compared to the nominal aircraft. On the rigid aircraft model, we showed through simulation that the right-half plane zero and its mirror image moved farther from the imaginary axis until they combined into a stable, although very lightly damped, complex-conjugate pair. A lower bound on the location of the right-half plane zero was established. In the case where flexibility effects were added to the model, the available bandwidth that could be achieved was limited due to complex coupling between the structural modes and the rigid body modes. In this case, the coupling usually produced a pair of mirror image complex-conjugate zeros; however, the additional control surface still showed an improved zero location, although it was more limited than in the rigid body case.

Acknowledgements

Part of this work was performed while the first author held a National Research Council Research Associateship Award at the Air Force Research Laboratory.

Appendix A Flight-Path Angle Transmission Zero Calculation

The non-linear, stability axis equations-of-motion for a rigid aircraft, written with respect to a flat earth, are

$$\dot{V}_T = \frac{T\cos\alpha - D}{m} - g\sin(\theta - \alpha) \tag{A.1}$$

$$\dot{\alpha} = -\frac{T\sin\alpha + L}{mV_T} + Q + \frac{g}{V_T}\cos(\theta - \alpha) \tag{A.2}$$

$$\dot{Q} = \frac{M}{I_{yy}} \tag{A.3}$$

$$\dot{h} = V_T\sin(\theta - \alpha) \tag{A.4}$$

$$\dot{\theta} = Q \tag{A.5}$$

where $M = M_{aero} + z_T T$ is the sum of the aerodynamic moments and the moment due to the thrust offset from the center-of-mass.

The linearized, stability axis equations-of-motion for the hypersonic aircraft are given below for a level, un-accelerated flight. We have assumed that $L_{\dot{\alpha}}$ and $M_{\dot{\alpha}}$ are negligible. The state vector is defined as

$$\boldsymbol{x} = \begin{bmatrix}\Delta V_T & \Delta\alpha & \Delta Q & \Delta h & \Delta\theta\end{bmatrix}^T \tag{A.6}$$

and the control vector is

$$\boldsymbol{u} = \begin{bmatrix}\Delta\delta_e & \Delta\delta_t\end{bmatrix}^T \tag{A.7}$$

The corresponding state matrix is given by

$$A = \begin{bmatrix} X_v & X_\alpha & 0 & X_h & -g \\ \frac{Z_v}{V_{T_0}} & \frac{Z_\alpha}{V_{T_0}} & \frac{1-Z_q}{V_{T_0}} & \frac{Z_h}{V_{T_0}} & 0 \\ M_v & M_\alpha & M_q & M_h & 0 \\ 0 & -V_0 & 0 & 0 & V_0 \\ 0 & 0 & 1 & 0 & 0 \end{bmatrix} \tag{A.8}$$

and the control influence matrix is

$$B = \begin{bmatrix} X_{\delta_e} & X_{\delta_t} \\ \frac{Z_{\delta_e}}{V_{T_0}} & \frac{Z_{\delta_t}}{V_{T_0}} \\ M_{\delta_e} & M_{\delta_t} \\ 0 & 0 \\ 0 & 0 \end{bmatrix} \tag{A.9}$$

The definitions of the stability and control derivatives for a hypersonic vehicle are different from their textbook definitions (see Stevens and Lewis[21] for example) because there are functional dependencies that are present for hypersonic aircraft that can be neglected for subsonic aircraft. The main driver being that air-breathing hypersonic aircraft have an engine that is highly integrated into the airframe. Thrust is now dependent upon angle-of-attack, in addition to Mach Number and altitude. The lift and pitching moment are now functions of the thrust setting in addition to the states (e.g., Q and α) and the elevator. Therefore, these relationships must be captured in the stability and control derivatives. For example,

$$X_\alpha = \frac{1}{m}\left(\frac{\partial T}{\partial \alpha}\cos\alpha_0 - \frac{\partial D}{\partial \alpha} + L_0\right) \tag{A.10}$$

where the subscript $()_0$ denotes the trim value of a particular variable. The complete set linearized stability and control derivatives for the hypersonic vehicle are found in Appendix B.

The linearized, stability axis equations-of-motion are in the following form

$$\dot{\boldsymbol{x}} = A\boldsymbol{x} + B\boldsymbol{u} \tag{A.11}$$

$$\boldsymbol{y} = C\boldsymbol{x} \tag{A.12}$$

where $\boldsymbol{x} \in \mathbb{R}^n$ and $\boldsymbol{u}$, $\boldsymbol{y} \in \mathbb{R}^m$. To compute the transmission zeros, it is necessary for the input, $\boldsymbol{u}$, to appear in the output equation. This requires differentiating the output equation with respect to time k times until the first non-zero Markov parameter, $CA^{k-1}B$, is found. For the linearized aircraft dynamics above with $\boldsymbol{y} = \begin{bmatrix}\gamma & V_t\end{bmatrix}^T$, the first non-zero Markov parameter is CB giving

$$\dot{\boldsymbol{y}} = CA\boldsymbol{x} + CB\boldsymbol{u} \tag{A.13}$$

Solving for $\boldsymbol{u}$ and substituting into Equation A.11 gives

$$\dot{\boldsymbol{x}} = (A - B(CB)^{-1}CA)\boldsymbol{x} + B(CB)^{-1}\dot{\boldsymbol{y}} \tag{A.14}$$

If CB is square and invertible, there are $n - m$ finite transmission zeros of the system (A, B, C). From El-Ghezawi,[22] the transmission zeros are given by the eigenvalues of $P^+ A_z P$

where P is the set of vectors that spans null(C), P^+ is the pseudo-inverse of P, and $A_z = A - B(CB)^{-1}CA$.

Literal expressions for the transmission zeros of the state-space system given by Equations A.11-A.12 can easily be found using any symbolic mathematics software package. The literal expression for the two non-zero transmission zeros for the above linearized aircraft dynamics is given by the following:

$$\begin{aligned} z_1, z_2 = \frac{1}{2}\Bigg[& M_q + \frac{(V_{T_0} + Z_q - 1)(M_{\delta_e} X_{\delta_t} - M_{\delta_t} X_{\delta_e})}{X_{\delta_t} Z_{\delta_e} - X_{\delta_e} Z_{\delta_t}} \pm \\ & \Bigg\{ \Big[(Z_q + V_{T_0} - 1)(M_{\delta_t} X_{\delta_e} - X_{\delta_t} M_{\delta_e}) - M_q (X_{\delta_t} Z_{\delta_e} - X_{\delta_e} Z_{\delta_t}) \Big]^2 - \\ & 4\big(X_{\delta_e} Z_{\delta_t} - X_{\delta_t} Z_{\delta_e}\big) \big[Z_\alpha (M_{\delta_t} X_{\delta_e} - M_{\delta_e} X_{\delta_t}) + (M_{\delta_t} Z_{\delta_e} - M_{\delta_e} Z_{\delta_t}) g + \\ & (M_\alpha X_{\delta_t} - M_{\delta_t} X_\alpha) Z_{\delta_e} + (M_{\delta_e} X_\alpha - M_\alpha X_{\delta_e}) Z_{\delta_t} \big] \Bigg\}^{1/2} (X_{\delta_t} Z_{\delta_e} - X_{\delta_e} Z_{\delta_t})^{-1} \Bigg] \end{aligned} \tag{A.15}$$

It should be noted that if one uses the full five state linearized equations-of-motion, such as those given in Equations A.8 and A.9, there will be a third transmission zero at the origin that corresponds to the climb rate equation.

Appendix B Stability and Control Derivatives for a Hypersonic Vehicle

The linearized, dimensional stability derivatives for a hypersonic vehicle are

$$M_V = \frac{1}{I_{yy}}\left(\frac{\partial M}{\partial V_T} + z_T\frac{\partial T}{\partial V_T}\right) \quad \text{(B.1)} \qquad Z_V = -\frac{1}{m}\left(\frac{\partial T}{\partial V_T}\sin\alpha_0 + \frac{\partial L}{\partial V_T}\right) \quad \text{(B.6)}$$

$$M_\alpha = \frac{1}{I_{yy}}\left(\frac{\partial M}{\partial \alpha} + z_T\frac{\partial T}{\partial \alpha}\right) \quad \text{(B.2)} \qquad Z_\alpha = -\frac{1}{m}\left(\frac{\partial T}{\partial \alpha} + D_0 + \frac{\partial L}{\partial \alpha}\right) \quad \text{(B.7)}$$

$$M_q = \frac{1}{I_{yy}}\frac{\partial M}{\partial Q} \quad \text{(B.3)} \qquad Z_q = -\frac{1}{m}\frac{\partial L}{\partial Q} \quad \text{(B.8)}$$

$$M_h = \frac{1}{I_{yy}}\left(\frac{\partial M}{\partial h} + z_T\frac{\partial T}{\partial h}\right) \quad \text{(B.4)} \qquad Z_h = -\frac{1}{m}\left(\frac{\partial T}{\partial h}\sin\alpha_0 + \frac{\partial L}{\partial \alpha}\right) \quad \text{(B.9)}$$

$$M_{\dot\alpha} = \frac{1}{I_{yy}}\frac{\partial M}{\partial \dot\alpha} \quad \text{(B.5)} \qquad Z_{\dot\alpha} = -\frac{1}{m}\frac{\partial L}{\partial \dot\alpha} \quad \text{(B.10)}$$

$$X_V = \frac{1}{m}\left(\frac{\partial T}{\partial V_T}\cos\alpha_0 - \frac{\partial D}{\partial V_T}\right) \quad \text{(B.11)}$$

$$X_\alpha = \frac{1}{m}\left(\frac{\partial T}{\partial \alpha}\cos\alpha_0 - \frac{\partial D}{\partial \alpha} + L_0\right) \quad \text{(B.12)}$$

$$X_h = \frac{1}{m}\left(\frac{\partial T}{\partial h}\cos\alpha_0 - \frac{\partial D}{\partial h}\right) \quad \text{(B.13)}$$

The control derivatives are

$$X_{\delta_e} = -\frac{1}{m}\frac{\partial D}{\partial \delta_e} \quad \text{(B.14)} \qquad Z_{\delta_e} = -\frac{1}{m}\frac{\partial L}{\partial \delta_e} \quad \text{(B.16)}$$

$$X_\phi = \frac{1}{m}\left(\frac{\partial T}{\partial \phi}\cos\alpha_0 - \frac{\partial D}{\partial \phi}\right) \quad \text{(B.15)} \qquad Z_\phi = -\frac{1}{m}\left(\frac{\partial T}{\partial \phi} + \frac{\partial L}{\partial \phi}\right) \quad \text{(B.17)}$$

$$M_{\delta_e} = \frac{1}{I_{yy}}\frac{\partial M}{\partial \delta_e} \quad \text{(B.18)}$$

$$M_\phi = \frac{1}{I_{yy}}\left(\frac{\partial M}{\partial \phi} + z_T\frac{\partial T}{\partial \phi}\right) \quad \text{(B.19)}$$

Note that there are several differences when compared to the traditional "textbook" definitions for the stability and control derivatives. The first is that the thrust is also a function of angle-of-attack. The dependency of thrust on angle-of-attack is present because the angle-of-attack, in conjunction with the flow turn angle of the forward fuselage, determines the angle of the oblique shock off of the nose of the aircraft. The residual effect is that not only does the pressure behind the shock change due to a change in angle-of-attack, the

mass flow entering the engine changes, both of which have an effect on the thrust. Second note that the dependence of the forces and the pitching moment on the equivalence ratio, ϕ, is included as the exhaust pressure acts on the lower aft fuselage of the aircraft and thus contributes to lift, drag, and the pitching moment. Furthermore, in Appendix A we assumed that $M_{\dot{\alpha}}$ and $L_{\dot{\alpha}}$ were negligible in our development of the literal expression for the transmission zeros, but are included here for completeness.

Appendix C Aircraft Configuration Data

The vehicle configuration data for the hypersonic vehicle model shown in Figure 14 and used in this study are as follows:

$$
\begin{aligned}
L &= 100 \text{ ft} & L_1 &= 47 \text{ ft} \\
\tau_{1_\ell} &= 6.2^\circ & L_b &= 20 \text{ ft} \\
\tau_{1_u} &= 3^\circ & \tau_2 &= 14.4^\circ \\
\bar{x} &= 55 \text{ ft} & h_{inlet} &= 3.25 \text{ ft} \\
c_t &= S_t/b = 17 \text{ ft} & x_c &= 5 \text{ ft} \\
m &= 300 \text{ slugs/ft} & x_t &= 85 \text{ ft} \\
I_{yy} &= 5 \times 10^5 \text{ slugs ft}^2/\text{ft} & z_t &= 3.5 \text{ ft}
\end{aligned}
$$

Note that the location of the control surfaces and the center-of-gravity are measured with respect to the nose of the aircraft. In this case the distance z_t is positive up and indicates that the hinge point of the elevator is 3.5 ft higher than the nose of the aircraft.

References

[1] Schmidt, D., "Integrated Control of Hypersonic Vehicles–A Necessity Not Just a Possibility," *Proceedings of the 1993 AIAA Guidance, Navigation, and Control Conference, Monterey CA*, Aug. 1993, pp. 539–549.

[2] Chavez, F. and Schmidt, D., "Analytical Aeropropulsive/Aeroelastic Hypersonic-Vehicle Model with Dynamic Analysis," *Journal of Guidance, Control, and Dynamics*,

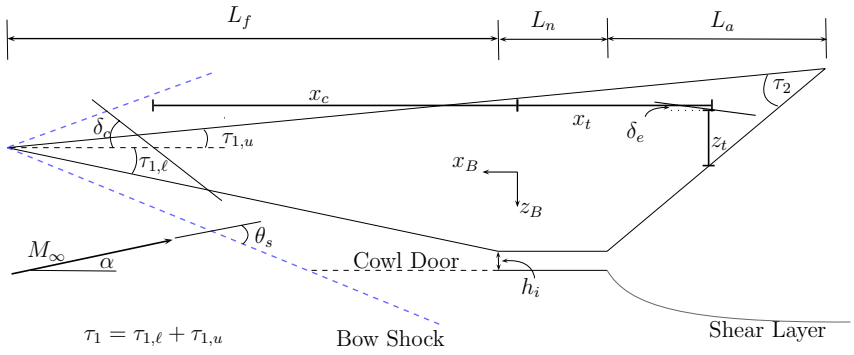

Figure 14: Hypersonic Air-breathing Vehicle Geometry

Vol. 17, No. 6, Nov./Dec. 1994, pp. 1308– 1319.

[3] Bolender, M. and Doman, D., "A Non-Linear Model for the Longitudinal Dynamics of a Hypersonic Air-breathing Vehicle," *Proceedings of the 2005 AIAA Guidance, Navigation, and Control Conference [CD-ROM]*, Aug 2005, AIAA 2005-6255.

[4] Sachs, G., "Longitudinal Long-Term Modes in Super- and Hypersonic Flight," *Journal of Guidance, Control, and Dynamics*, Vol. 28, No. 3, May/June 2005, pp. 539–541.

[5] Stengel, R., "Altitude Stability in Supersonic Cruising Flight," *Journal of Aircraft*, Vol. 7, No. 9, Sept./Oct. 1970, pp. 464–473.

[6] Sachs, G., "Increase and Limit of T_{θ_2} in Super- and Hypersonic Flight," *Journal of Guidance, Control, and Dynamics*, Vol. 22, No. 1, Jan./Feb. 1999, pp. 181–183.

[7] Roskam, J., *Airplane Flight Dynamics and Automatic Flight Control*, Vol. I, Roskam Aviation and Engineering Corp., Lawrence, KS, 1982, pp. 607–615.

[8] Heffley, R. and Jewell, W., "Aircraft Handling Qualities Data," Tech. Rep. NACA-CR-2144, NASA, Washington, DC 20546, December 1972.

[9] "Military Standard 1797A Flying Qualities of Piloted Aircraft," Tech. rep., USAF ASD/ENES, Wright-Patterson AFB, OH, 1990.

[10] Sachs, G., "Path-Attitude Decoupling and Flying Qualities Implications in Hypersonic Flight," *Aerospace Science and Technology*, Vol. 2, No. 1, Jan. 1998, pp. 49–59.

[11] Bloy, A., "Thrust Offset Effect on Longitudinal Dynamic Stability," *Journal of Aircraft*, Vol. 35, No. 2, Mar./Apr. 1998, pp. 343–344.

[12] Berry, D., "National Aerospace Plane Flying Qualities Task Definition Study," Tech. Rep. NASA TM-1039, NASP/JPO, 1989.

[13] Berry, D., "National Aerospace Plane Flying Qualities," Tech. Rep. NASA TM-1084, NASP/JPO, 1989.

[14] McRuer, D., Myers, T., Hoh, R., Ashkenas, I., and Johnston, D., "Assessment of Flying Quality Criteria for Air-breathing Aerospacecraft," Tech. Rep. NASA-CR-4442, NASA Dryden Flight Research Facility, 1992.

[15] Vu, P. and Biezad, D., "Direct-Lift Design Strategy for Longitudinal Control of Hypersonic Aircraft," *Journal of Guidance, Control, and Navigation*, Vol. 17, No. 6, Nov./Dec. 1994, pp. 1260–1266.

[16] McRuer, D. T., Ashkenas, I., and Graham, D., *Aircraft Dynamics and Automatic Control*, chap. 5, Princeton University Press, Princeton, NJ, 1973, pp. 336–337.

[17] Field, E., Armor, J., Rossitto, K., and Mitchell, D., "Effects of Instantaneous Center of Rotation Location on Flying Qualities," *Proceedings of the AIAA Atmospheric Flight Mechanics Conference [CD-ROM]*, Aug. 5-8 2002, AIAA 2002-4799.

[18] Maciejowski, J., *Multivariable Feedback Design*, Addison-Wesley, 1989, pp. 27–34.

[19] Stein, G., "Respect the Unstable," *IEEE Control Systems Magazine*, Vol. 23, No. 4, August 2003, pp. 12–25.

[20] Lindner, D., Reichard, K., and Tarkenton, L., "Zeros of Modal Models of Flexible Structures," *IEEE Transactions on Automatic Control*, Vol. 38, No. 9, Sept.

[21] Stevens, B. and Lewis, F., *Aircraft Control and Simulation*, Wiley and Sons, Hoboken, N.J., 2nd ed., 2003, pp. 120–131.

[22] El-Ghezawi, O., Zinober, A., Owens, D., and Billings, S., "Computation of the Zeros and Zero Directions of Linear Multivariable Systems," *International Journal of Control*, Vol. 36, No. 5, Nov. 1982, pp. 833–843.